ACS OMEGA

http://pubs.acs.org/journal/acsodf

Article

Role of Hydrogen in Catalyst Activation for Plasma-Based Synthesis of Carbon Nanotubes

Takashi Tsuji, Jaeho Kim, Hajime Sakakita, Yoshiki Shimizu, Guohai Chen, Kenji Hata, Don N. Futaba,* and Shunsuke Sakurai*

Cite This: *ACS Omega* 2021, 6, 18763−18769

Read Online

ACCESS | Metrics & More | Article Recommendations | Supporting Information

ABSTRACT: The importance of hydrogen in carbon nanotube (CNT) synthesis has been known as it supports the critical processes necessary for CNT growth, such as catalyst reduction. However, within the scope of our mini microplasma CNT synthesis reactor, we found that hydrogen was critical for unexpected reasons. Without hydrogen, CNT growth was inhibited and characterized by amorphous carbon particles. Optical emission spectroscopy of the microplasma revealed that without hydrogen, the high-energy electrons induced the immediate decomposition of carbon feedstock simultaneously with the catalyst feedstock, thus suppressing the formation of catalyst nanoparticles and inducing catalyst deactivation. In contrast, the inclusion of hydrogen induced less-immediate decomposition of reactant gases, through the conversion of electron energy of the plasma to thermal energy, which provided the appropriate conditions for catalyst nanoparticle formation and subsequent CNT nucleation. A simple reaction pathway model was proposed to explain these observed results and underlying mechanisms.

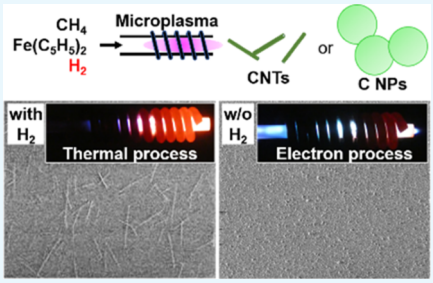

INTRODUCTION

Hydrogen (H_2) is well known as a vital process gas for the synthesis of carbon nanotubes (CNTs).[1−10] H_2 has been well-documented for the reduction and formation of the catalyst nanoparticle to serve as active sites for CNT growth for thermal-based chemical vapor deposition (CVD) methods.[3−5] In addition, numerous reports further show that H_2 can promote synthesis during the growth phases as well. For example, it can act as an etchant to maintain a reduced oxidation state of the catalyst surface during the growth phase and thereby prevent catalyst poisoning.[7] In addition, it has been reported that H_2 can drive a defect healing process during the formation of the polycyclic aromatic hydrocarbons.[11] H_2 has also been reported to be important for plasma-based physical vaporization processes, such as arc discharge[8,9] and inductively coupled plasma.[10] For example, the use of H_2 in the reactive gases for multiwalled CNT production by arc discharge has been reported to be more effective than an inert ambient due to the higher temperature and high activity of the H_2 arc.[12] In addition, Kim et al. also described that H_2 plasma contributed to the purity improvement.[10] Therefore, H_2 has shown to play a critically important role to support the growth of CNTs in various growth ambients.

Methane (CH_4) is often used as a carbon feedstock for CNT synthesis.[13−15] Because CH_4 is a very stable molecule with strong C−H bonds and high symmetry, it requires significant energy, for example, high temperatures, for pyrolysis, and numerous approaches have been reported revealing different reaction pathways. To reduce the necessary reaction temperature, transition metal catalysts due to their partially filled 3d orbitals (commonly Iron (Fe)) are used to serve as active sites to aid in the dehydrogenation of CH_4.[16] As a result, hydrogen and CH_x are formed, which eventually result in the production of higher hydrocarbons (such as acetylene, ethylene, ethane, etc.). In the case of plasmas, high energy electron impact is highly effective in the dissociation of the CH_4 molecules.[17] In this case, upon entering the plasma, the hydrogen atoms are removed from the methane to form a reactive carbon species. However, depending on the thermal properties of the plasma, these reactant species can follow different pathways as shown by Lee et al.[18] In cold plasmas, the primary product is C_2H_6, while in contrast, in "warmer" plasmas, most products were dimer forms of carbon, such as ethane, acetylene, ethylene. This is significant as acetylene has been reported to be one of the primary precursors for CNT synthesis.[19−21] When the Fe particles with appropriate size are present, CNTs can nucleate and grow from the particles in both thermal-[14,22] and plasma-based processes[23] using a CH_4 feedstock. In such cases, Fe particles can act for both catalyzing CH_4 activation (especially for the thermal CVD) and for providing a nanoscale template for the nucleation and growth of CNTs.[24] In the case of

Received: April 6, 2021
Accepted: July 6, 2021
Published: July 14, 2021

plasma-enhanced CVD approaches,[25] heating of the Fe particles is also necessary to supply the activation energy for the CNT nucleation and growth reaction.

In a previous report, we demonstrated a mini synthesis reactor using microplasma as the sole energetic component.[26] Small enough to fit within the palm of one's hand, we demonstrated that the microplasma could be used to perform all the necessary functions for CNT synthesis, such as catalyst feedstock decomposition, carbon feedstock decomposition, nanoparticle formation, and CNT nucleation and growth (Figure 1). By flowing all of the reactant gases through the microplasma capillary, analogous to that of a furnace, this mini synthesis reactor demonstrated continuous flow and gas-phase synthesis of highly crystalline (graphitic-to-disorder band intensity ratio: ~100) and small-diameter (~2 nm) single- and double-walled CNTs at an exceptionally high growth rate. In this current experiment, ferrocene ($FeCp_2$) and CH_4 were used for the precursors of Fe catalyst nanoparticles and CNTs, respectively. Conventional understanding on the reaction pathway of the gas-phase CNT synthesis is that catalyst precursors ($FeCp_2$) are first decomposed and the Fe nucleates into catalyst nanoparticles and then decomposition of the CH_4 on the formed Fe catalyst nanoparticles promotes the nucleation and growth of CNTs.[14] The catalytic reaction of CH_4 on nanoparticles is inactivated mainly due to coking or carbon deposition on catalyst nanoparticles.[13,27] To prevent coke formation, various methods, such as the addition of hydrogen and use of single metal atom or bimetallic particle catalysts, have been developed.[28−30] In our microplasma reactor, H_2 was found to be an important process gas for the synthesis of CNTs but not for the previously reported reasons.

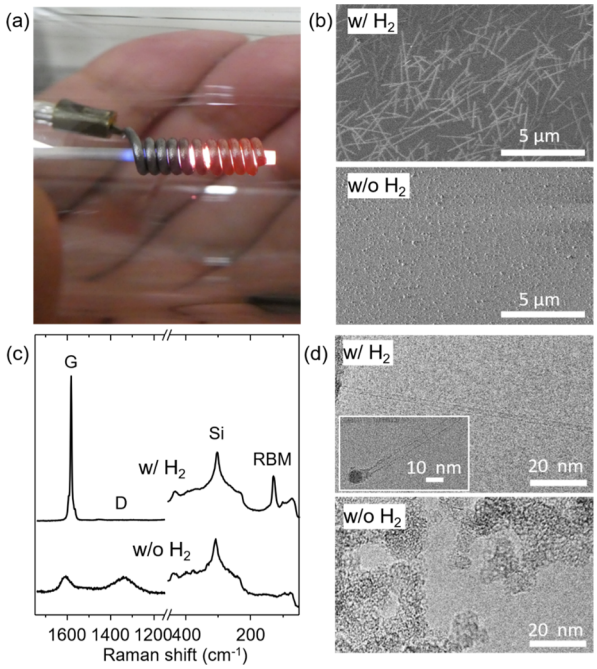

Figure 1. (a) Photograph of the microplasma reactor, (b) SEM images, (c) Raman spectra, and (d) TEM images of the products grown with and without H_2.

Here, we report the role of H_2 on the formation of Fe catalyst nanoparticles responsible for the synthesis of CNTs from $FeCp_2$ and CH_4 in the microplasma reactor. Our results showed that without H_2, the decomposition process of reactant species was dominated by the electron impact from the argon (Ar) plasma. As a result, decomposition of the reactant species ($FeCp_2$ and CH_4) simultaneously occurred, which inhibited the nucleation of Fe nanoparticles. The absence of Fe catalyst nanoparticles led to the formation of amorphous carbon particles as the primary synthesis products as observed by transmission electron microscopy (TEM). In contrast, with the inclusion of H_2 into the reactant gas flow, the generation of amorphous carbon particles was replaced with highly crystalline and straight CNTs. Optical emission spectroscopy (OES) investigation revealed that H_2 acted to promote thermal reaction pathways by acting as a medium to convert the plasma electron energy into thermal energy, through electronic excitation of H_2 molecules and its nonradiative relaxation. Thus, a thermal component for the decomposition of the reactant species was introduced, whose order was governed by their respective dissociation energies. Therefore, we interpret that Fe catalyst nanoparticles were able to nucleate and act as precipitation sites for the formation of CNTs. Based on these experimental results, a simple reaction pathway schematic was proposed to explain the underlying mechanisms and results.

RESULTS AND DISCUSSION

To begin, we investigated the effect of H_2 in the reactant gases on the microplasma synthesis of carbon nanomaterials. A microplasma was generated using a ceramic capillary with an Ar flow which was surrounded by a coiled electrode supplied with ultrahigh frequency (UHF) power (450 MHz). Synthesis was conducted by introducing $FeCp_2$ (~0.001%) catalyst feedstock, CH_4 (0.16%) carbon feedstock, and H_2 (5%) into the Ar carrier gas flow (total flow rate: 150 sccm) for 1 min. Products were directly deposited onto a silicon wafer with a thermally oxidized layer. As a reference, synthesis without H_2 was also conducted. With H_2, exceptionally straight and fibrous materials were observed using scanning electron microscopy (SEM; Hitachi S-4800) images (Figure 1b, upper panel). Both Raman spectroscopy (Horiba; XploRA) and TEM (TOPCON EM-002B) of the products confirmed high crystallinity of the CNTs. Specifically, Raman spectroscopy with 532 nm excitation wavelength exhibited a strong Raman graphitic (G) band, a negligibly weak disorder (D) band, and radial breathing mode peaks, which indicated the production of highly crystalline CNTs (Figure 1c). TEM observation further showed highly straight CNTs, primarily single-wall and double-wall, with an average diameter of 2 nm (Figure 1d, upper panel). TEM observation also showed CNTs connected to the catalyst nanoparticles, which is evidence that the CNT growth was catalyzed by the nanoparticle (inset of Figure 1d). This point is important in understanding the role of H_2. Interestingly, CNTs were observed to grow by a "perpendicular" growth mode, where the diameter is smaller than that of the catalyst particle size. This observation differs from the results from thermal catalyst CVD also using a CH_4 feedstock where the "tangential" growth mode was observed.[31] This indicates that the use of the plasma partially alters the growth mode selection. In contrast, without H_2, the synthesis was characterized by the absence of CNTs and an abundance of aggregated spherical nanoparticles (Figure 1b, lower panel). Raman spectra of the nanoparticles showed broad G and D bands with a G/D ratio of ~1 (Figure 1c), which is typical of disordered carbon.[32] TEM images showed the amorphous carbon particles with a diameter of ~10 nm (Figure 1d, lower panel). Importantly, we did not observe the presence of Fe

https://doi.org/10.1021/acsomega.1c01822
ACS Omega 2021, 6, 18763−18769

catalyst nanoparticles, which would suggest that the formation of Fe particles large enough to observe in our experimental condition did not occur. This result indicated that the presence of H_2 is critical for the formation of Fe catalyst nanoparticles and the nucleation and growth of CNTs.

A visible difference in the plasma could be observed in the color and appearance with and without the inclusion of H_2 (insets of Figure 2a). Without H_2, the plasma jet extending

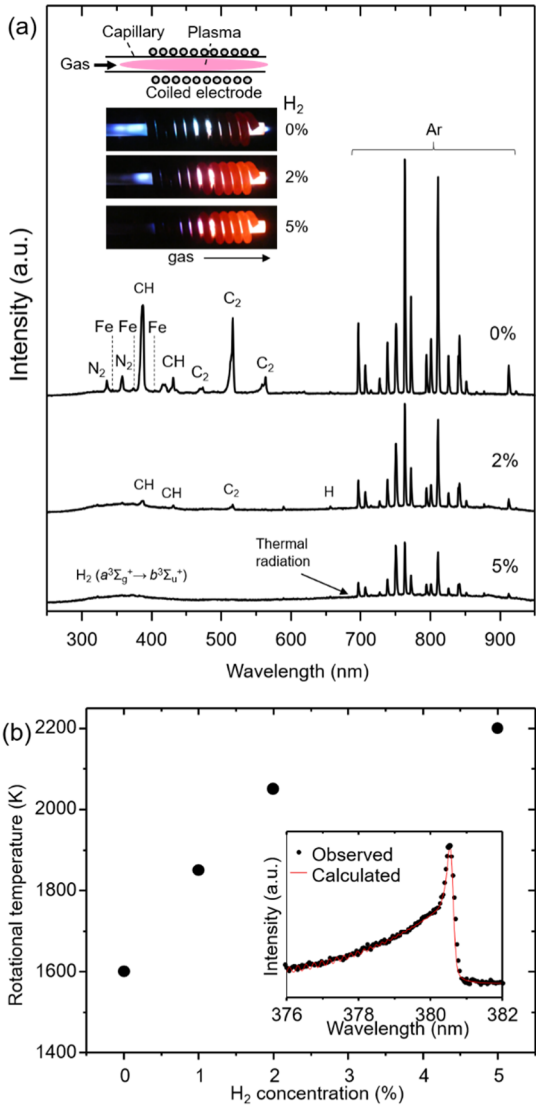

Figure 2. (a) Optical emission spectra of the microplasma with different concentrations of H_2. The inset shows the schematic diagram illustrating the microplasma reactor and the photographs of the microplasma with different H_2 concentrations. (b) Gas temperature characterized as the rotational temperature of N_2 molecules as a function of H_2 concentration. The inset shows the observed and calculated N_2 second positive system (SPS) bands for a H_2 concentration of 0%.

~0.5 mm outside of the capillary appeared as white-blue, the blue plasma was visible on both ends of the coil, and the plasma coil is dull orange. In contrast, when H_2 is at 2%, the plasma jet is noticeably shorter, the blue plasma region is shortened, and the plasma coil has a strong orange color. When 5% H_2 is included to the flow gases, the plasma jet is no longer visibly extending outside of the capillary, the blue plasma is no longer visible as it is behind the coil, and the coil, itself, is a slightly brighter shade of orange. This visible color difference indicates that contents of the emitted plasma gases differed in the three cases. To elucidate the effect of H_2 on the decomposition of the feedstocks [$FeCp_2$ (~0.001%) and CH_4 (~0.16%)] passing through the microplasma, the contents of the plasma were examined by OES.

The OES spectra (Ocean Optics, FLAME-S-XR1) measured at the middle of the microplasma capillary revealed significant changes by the addition of H_2. Using a pure Ar carrier gas (no H_2), the OES spectra showed clear and sharp Ar transitions (690−930 nm) and emission bands of CH (386 and 431 nm), C_2 (473, 516, and 563 nm), and Fe (344, 374, and 404 nm). This result indicates that the $FeCp_2$ and CH_4 feedstocks were both effectively decomposed to atomic Fe, CH, and C_2 radicals by passage through the plasma (Figure 2a). Note that the presence of N_2 (336 and 357 nm) emission is likely due to plasma generated at the outside of the capillary or a background presence of N_2 impurity inside the gas lines because N_2 was not intentionally included inside the capillary.

In contrast, when H_2 (2 and 5%) was added to the microplasma carrier gas, the relative intensities of the CH, C_2, and Fe emission bands were significantly decreased with increased H_2 concentrations (Figure 2a). Emission bands from CH and C_2 were weakly observed when H_2 concentration was 2%, but they became nearly undetectable when the H_2 concentration reached 5%. Note: as discussed later, the reduction in CH and C_2 emission bands only indicates the reduction of electron-induced formation of these radicals. In addition, two strong and broad emission bands were observed in ~380 and ~>600 nm. The broad band at ~380 nm can be assigned to the $a^3\Sigma_g^+ \rightarrow b^3\Sigma_u^+$ transition of the H_2 molecule.[33] The observation of the H_2 $a^3\Sigma_g^+ \rightarrow b^3\Sigma_u^+$ transition indicates that the Ar plasma excited the H_2 molecule from the ground state to the $a^3\Sigma_g^+$ state, which then relaxed via emission to the $b^3\Sigma_u^+$ state. Because the $b^3\Sigma_u^+$ state is a dissociative electronic state,[33] this result indicates that H_2 molecules were dissociated into atomic H. As the atomic H recombined to reform H_2 molecules, heat was generated, which led to the observed increase in gas temperature of the plasma, as evidenced by the analysis of the N_2 SPS band discussed later. The broad band observed at >600 nm can be assigned as thermal radiation from the capillary.

The gas temperature was estimated from the rotational temperature of N_2 molecules by fitting the SPS of the N_2 molecule. This estimation is expected to be accurate because the rotational temperature of molecules in the atmospheric pressure plasma is close to the gas temperature of the plasma.[34] The N_2 SPS bands were obtained by OES using a high-resolution spectrometer (HR4000; Figure S2). For this experiment, a small amount of N_2 (1%) was intentionally added to the microplasma gas flow at different concentrations of H_2 (0, 1, 2, and 5%) with Ar (total flow: 150 sccm) to obtain the N_2 SPS peaks. The rotational temperatures of N_2 were estimated by fitting the experimentally observed spectra of the SPS with a numerical model as shown in the inset of Figure 2b. The estimated rotational temperatures of N_2 were found to monotonically increase with the H_2 concentration as it was increased from 0 to 5% and approach a maximum of ~2200 K (Figure 2b). Taken together, these results indicate that H_2 acted as a medium that converts plasma electron energy into thermal energy, and in doing so, it promotes the thermal reaction pathways in place of the electron process.

https://doi.org/10.1021/acsomega.1c01822
ACS Omega 2021, 6, 18763−18769

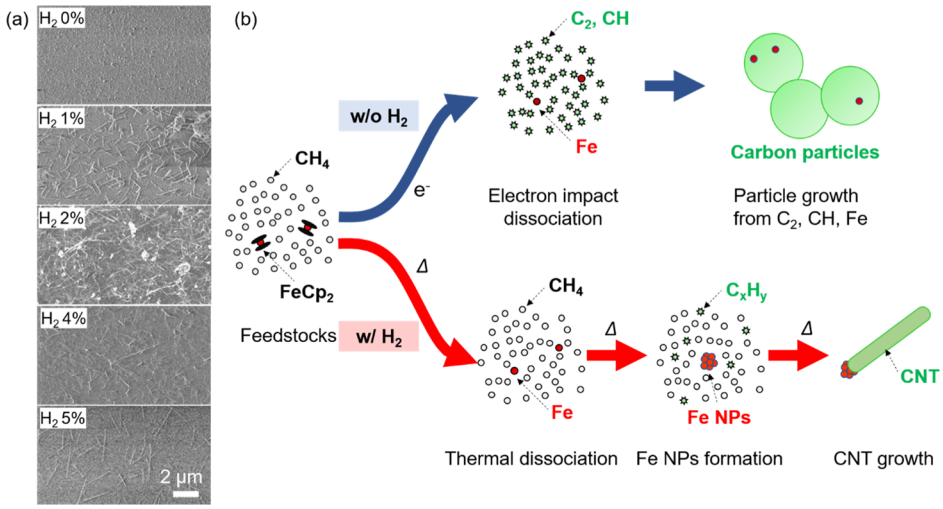

Figure 3. (a) SEM images of the product with different H_2 concentrations. (b) Proposed model of the reaction pathways in microplasma synthesis with and without H_2.

The CNT growth exhibited a clear dependence on the concentration of H_2, as shown in Figure 3a. As previously described, with zero H_2, the CNT yield was not apparent and characterized by the preponderance of amorphous carbon particles. As the H_2 concentration was increased, we observed an increase in the amount of CNT production. Interestingly, we observed the highest level of CNT production that occurred at ∼2% H_2 concentration and a slightly decreased production as the H_2 concentration was increased to 5%. Correspondingly, the amount of amorphous carbon particles monotonically decreased with H_2 concentration, which also correlated with the increased Raman G/D ratio, as shown in Figure S1. These results indicate that the CH_4 fragments, such as C_2 and CH, produced by electron impact in the plasma aggregated to form amorphous carbon particles in the absence of H_2. By increasing the H_2 concentration, the reaction pathway shifted from that of amorphous carbon particles (blue line, Figure 3b) to CNT synthesis (red line, Figure 3b) as the dissociation process shifted from that of a purely electron impact process to include a thermal process.

Based on these results, we propose a simple model on the role of H_2 in the synthesis of CNTs (Figure 3b). To begin, we specify the basic stages and order for CNT synthesis as (1) decomposition of the catalyst feedstock, (2) nucleation and growth of the catalyst nanoparticles, (3) decomposition of the carbon feedstock, and (4) nucleation and growth of the CNT.

When H_2 is not present, the reaction follows a "no CNT growth" pathway. The input $FeCp_2$ and CH_4 (concentration ratio of 1:100) are simultaneously decomposed by the electron impact in the microplasma to produce C_2, CH, and Fe, as evidenced by the emission spectra (Figure 2a). We interpret that the presence of the decomposed carbon feedstock with the decomposed catalyst feedstock hinders the formation of Fe nanoparticles and, as observed, forms clusters of carbon with atomic-scale Fe within. This is plausible because the amount of C is 100 times larger than Fe. Due to the absence of formed Fe catalyst nanoparticles to act as reaction sites, the carbon species form large amorphous carbon aggregates as seen in the TEM images (Figure 1d). These carbon particles likely contain Fe atoms or small clusters, but due to the small size, they were not observed in TEM images, that is, lack of opaque features.

In contrast, when H_2 is present, the reaction follows the "CNT growth" pathway. As evidenced by the OES results (Figure 2), plasma electron energy is not used solely to directly dissociate the catalyst and carbon feedstocks but rather for the H_2 molecule excitation and associated temperature increase. Thus, we observed decreased emission intensities of C_2 and CH radicals from CH_4 and Fe atoms from $FeCp_2$ in the OES spectra (Figure 2a). In this case, we interpret that decomposition of both the $FeCp_2$ and CH_4 are thermally activated rather than electron impact. The reaction rate of the thermal decomposition is known to follow the Arrhenius equation ($k = A\exp(-E/RT)$), where k is the rate constant, A is the pre-exponential factor, R is the universal gas constant, T is the absolute temperature, and E is the activation energy (dissociation energy), and $FeCp_2$ is expected to decompose before CH_4 due to the difference in dissociation energies ($EFeCp_2 < ECH_4$). Therefore, in this situation, the catalyst nanoparticles could nucleate prior to the pyrolysis of CH_4 to support the nucleation and growth of CNTs. In short, H_2 in the plasma increased the gas temperature which supports the thermal-driven decomposition of the feedstocks and the promotion of the CNT growth process.

Our results further show that the relative peak in the CNT yield observed at 2% H_2 is followed by a decrease at 5% (Figure 3a). We believe that two basic factors could contribute to the decrease in CNT yield by the addition of excess H_2. First, the reduction in the CNT growth time due to increased plasma temperature could affect the CNT yield. As the H_2 concentration is increased, the local gas temperature in the microplasma is also increased as 1600, 1850, 2050, and 2200 K for 0, 1, 2, and 5% H_2, respectively (Figure 2b). The pressure of the Fe vapor converted from $FeCp_2$ (∼1 Pa) should be well below the saturation vapor pressure of Fe at the observed high temperature (∼170 Pa for 2200 K). In this case, the catalyst nanoparticle nucleation cannot occur until after the decomposed species have exited the capillary. Therefore, because the formation of the catalyst nanoparticle occurs later, the time in the carbon-rich environment is shorter, resulting in fewer CNTs at H_2 concentration higher than 2%. Second, based on the chemical equilibrium of the well-known reaction, $CH_4 \leftrightarrow C_{CNT} + 2H_2$, the increase in H_2 could promote a reverse

https://doi.org/10.1021/acsomega.1c01822
ACS Omega 2021, 6, 18763−18769

reaction to inhibit CH_4 decomposition and reduced the formation of CNTs.

Comparison with previous reports on the use of hydrogen in plasma-based CNT synthesis reactors highlights the novelty of the role of hydrogen in our system. Previous reports showed that the presence of H_2 in the plasma-based CNT synthesis ambient increase yield and purity by keeping the catalyst surface active by etching the encapsulating carbon and etching the impurities of amorphous carbon by forming hydrocarbons.[35,36] We expect that the etching reaction also occurs to some extent in our microplasma reactor in the presence of H_2. However, a decrease in the CH and C_2 peaks by the addition of H_2 observed in OES spectra (Figure 2a), which we attributed to the shift of decomposition from electron-driven to thermally driven processes, could not be explained by the abovementioned etching reaction. Therefore, our study provides additional understanding of the role of hydrogen in reducing the active carbon species forming unwanted amorphous carbon by suppressing the electron impact decomposition of carbon feedstocks for the formation of the active catalyst nanoparticles.

CONCLUSIONS

In conclusion, we have demonstrated the importance and role of H_2 for our microplasma synthesis of highly crystalline CNTs. Our results showed that H_2, in contrast to other reports, aids in the growth of CNTs through inducing a shift in the dissociation process of the feedstock gases from that of a solely electron process to a thermal process through the conversion of plasma electron energy into thermal energy by the dissociation and recombination of the H_2 molecules. This shift allows the appropriate order for the CNT synthesis where decomposition of catalyst feedstock ($FeCp_2$) and the formation of Fe catalyst nanoparticles followed by decomposition of carbon feedstock (CH_4) and the formation of CNTs, whereas, without H_2, electron impact in the plasma decomposed the carbon and catalyst feedstocks simultaneously, which results in the formation of amorphous carbon nanoparticles without the formation of Fe catalyst nanoparticles. These results demonstrate that H_2 acts as a "support" gas to modulate the dissociation process and highlights the importance in the sequence of stages necessary for CNT synthesis.

EXPERIMENTAL SECTION

Microplasma Generation. The microplasma reactor is composed of an alumina ceramic capillary (1.2 mm outer diameter and 0.8 mm inner diameter) surrounded by a φ1 mm tantalum (Ta) wire coil with 10 turns. A tungsten wire (φ0.2 mm) was inserted inside the capillary as a counter electrode. For plasma generation, Ar was flowed through the capillary while supplying 450 MHz UHF power to the Ta coil (30 W) using the 450 MHz/100 W high-frequency power source (J S Engineering Co. Ltd).

Synthesis of Carbon Nanomaterials. For the synthesis of carbon nanomaterials, Ar-based mixed gas (150 sccm) including CH_4 (0.16%) and H_2 (0−5%) passed through a $FeCp_2$ cartridge at room temperature and was supplied to the microplasma reactor. $FeCp_2$ concentration in the mixed gas was estimated to be ∼0.001% from the saturated vapor pressure of the $FeCp_2$. Microplasma was then generated for 1 min by supplying UHF power (30 W) to initiate nanocarbon synthesis. The product was collected onto a silicon substrate with a thermally oxidized layer (SiO_2/Si) or TEM grids (NS-C15 from Okenshoji Co. Ltd. or US100-A05Q33A from ALLIANCE Biosystems) placed at 15 mm downstream of the capillary outlet.

Characterization. The products were characterized by SEM (Hitachi, S-4800), Raman spectroscopy (Horiba, XploRA) with 532 nm excitation wavelength, and TEM (TOPCON EM-002B).

Optical Emission Spectroscopy. OES of the microplasma was performed using FLAME-S-XR1 (Ocean Optics) with a resolution of 1.75 nm at full width at half-maximum (FWHM) or HR4000 (Ocean Optics) with a resolution of 0.17 nm at FWHM. The emission from the middle of the microplasma was collected using a lens and guided to the spectrometer by an optical fiber.

ASSOCIATED CONTENT

Supporting Information

The Supporting Information is available free of charge at https://pubs.acs.org/doi/10.1021/acsomega.1c01822.

Raman spectra of the CNTs grown with different hydrogen concentrations and experimentally observed spectra of the (0−2) region for the SPS of N_2 at different concentrations of H_2 (0, 1, 2, and 5%) and calculated curves for 1600, 1850, 2050, and 2200 K (PDF)

AUTHOR INFORMATION

Corresponding Authors

Don N. Futaba − *CNT-Application Research Center, National Institute of Advanced Industrial Science and Technology (AIST), Tsukuba, Ibaraki 305-8565, Japan;* orcid.org/0000-0002-7083-2772; Phone: +81-29-861-4654; Email: d-futaba@aist.go.jp

Shunsuke Sakurai − *CNT-Application Research Center, National Institute of Advanced Industrial Science and Technology (AIST), Tsukuba, Ibaraki 305-8565, Japan;* orcid.org/0000-0002-0465-3274; Phone: +81-29-861-4654; Email: shunsuke-sakurai@aist.go.jp

Authors

Takashi Tsuji − *CNT-Application Research Center, National Institute of Advanced Industrial Science and Technology (AIST), Tsukuba, Ibaraki 305-8565, Japan;* orcid.org/0000-0003-2915-1841

Jaeho Kim − *Innovative Plasma Processing Group, Research Institute for Advanced Electronics and Photonics, National Institute of Advanced Industrial Science and Technology (AIST), Tsukuba, Ibaraki 305-8568, Japan;* orcid.org/0000-0001-7365-7319

Hajime Sakakita − *Innovative Plasma Processing Group, Research Institute for Advanced Electronics and Photonics, National Institute of Advanced Industrial Science and Technology (AIST), Tsukuba, Ibaraki 305-8568, Japan*

Yoshiki Shimizu − *Nanomaterials Research Institute, National Institute of Advanced Industrial Science and Technology (AIST), Tsukuba, Ibaraki 305-8565, Japan; AIST-UTokyo Advanced Operando-Measurement Technology Open Innovation Laboratory (OPERANDO-OIL), National Institute of Advanced Industrial Science and Technology (AIST), Kashiwa, Chiba 227-8589, Japan*

https://doi.org/10.1021/acsomega.1c01822
ACS Omega 2021, 6, 18763−18769

Guohai Chen − *CNT-Application Research Center, National Institute of Advanced Industrial Science and Technology (AIST), Tsukuba, Ibaraki 305-8565, Japan;* orcid.org/0000-0001-8481-0972

Kenji Hata − *CNT-Application Research Center, National Institute of Advanced Industrial Science and Technology (AIST), Tsukuba, Ibaraki 305-8565, Japan*

Complete contact information is available at: https://pubs.acs.org/10.1021/acsomega.1c01822

Notes

The authors declare no competing financial interest.

■ ACKNOWLEDGMENTS

We would like to acknowledge the technical assistance from M. Yamada, M. Irie, and J. He.

■ REFERENCES

(1) Li, Y.-L.; Kinloch, I. A.; Windle, A. H. Direct Spinning of Carbon Nanotube Fibers from Chemical Vapor Deposition Synthesis. *Science* **2004**, *304*, 276−278.

(2) Skukla, B.; Saito, T.; Ohmori, S.; Koshi, M.; Yumura, M.; Iijima, S. Interdependency of Gas Phase Intermediates and Chemical Vapor Deposition Growth of Single Wall Carbon Nanotubes. *Chem. Mater.* **2010**, *22*, 6035−6043.

(3) Ding, E.-X.; Hussain, A.; Ahmad, S.; Zhang, Q.; Liao, Y.; Jiang, H.; Kauppinen, E. I. High-Performance Transparent Conducting Films of Long Single-Walled Carbon Nanotubes Synthesized from Toluene Alone. *Nano Res.* **2020**, *13*, 112−120.

(4) Page, A. J.; Saha, S.; Li, H.-B.; Irle, S.; Morokuma, K. Quantum Chemical Simulation of Carbon Nanotube Nucleation on Al2O3 Catalysts via CH4 Chemical Vapor Deposition. *J. Am. Chem. Soc.* **2015**, *137*, 9281−9288.

(5) Mitchell, I.; Page, A. J. The Influence of Hydrogen on Transition Metal - Catalysed Graphene Nucleation. *Carbon* **2018**, *128*, 215−223.

(6) Hoecker, C.; Smail, F.; Bajada, M.; Pick, M.; Boies, A. Catalyst Nanoparticle Growth Dynamics and Their Influence on Product Morphology in a CVD Process for Continuous Carbon Nanotube Synthesis. *Carbon* **2016**, *96*, 116−124.

(7) Page, A. J.; Ding, F.; Irle, S.; Morokuma, K. Insights into Carbon Nanotube and Graphene Formation Mechanisms from Molecular Simulations: A Review. *Rep. Prog. Phys.* **2015**, *78*, 036501.

(8) Zhao, X.; Ohkohchi, M.; Wang, M.; Iijima, S.; Ichihashi, T.; Ando, Y. Preparation of High-Grade Carbon Nanotubes by Hydrogen Arc Discharge. *Carbon* **1997**, *35*, 775−781.

(9) Wang, X. K.; Lin, X. W.; Dravid, V. P.; Ketterson, J. B.; Chang, R. P. H. Carbon Nanotubes Synthesized in a Hydrogen Arc Discharge. *Appl. Phys. Lett.* **1995**, *66*, 2430−2432.

(10) Kim, K. S.; Kingston, C. T.; Ruth, D.; Barnes, M.; Simard, B. Synthesis of High Quality Single-Walled Carbon Nanotubes with Purity Enhancement and Diameter Control by Liquid Precursor Ar-H_2 plasma Spraying. *Chem. Eng. J.* **2014**, *250*, 331−341.

(11) Li, H.-B.; Page, A. J.; Irle, S.; Morokuma, K. Revealing the Dual Role of Hydrogen for Growth Inhibition and Defect Healing in Polycyclic Aromatic Hydrocarbon Formation: QM/MD Simulations. *J. Phys. Chem. Lett.* **2013**, *4*, 2323−2327.

(12) Ando, Y.; Zhao, X.; Sugai, T.; Kumar, M. Growing Carbon Nanotubes. *Mater. Today* **2004**, *7*, 22−29.

(13) Dong, Z.; Li, B.; Cui, C.; Qian, W.; Jin, Y.; Wei, F. Catalytic Methane Technology for Carbon Nanotubes and Graphene. *React. Chem. Eng.* **2020**, *5*, 991−1004.

(14) Gspann, T. S.; Smail, F. R.; Windle, A. H. Spinning of Carbon Nanotube Fibres Using the Floating Catalyst High Temperature Route: Purity Issues and the Critical Role of Sulphur. *Faraday Discuss.* **2014**, *173*, 47−65.

(15) Okada, S.; Sugime, H.; Hasegawa, K.; Osawa, T.; Kataoka, S.; Sugiura, H.; Noda, S. Flame-Assisted Chemical Vapor Deposition for Continuous Gas-Phase Synthesis of 1-Nm-Diameter Single-Wall Carbon Nanotubes. *Carbon* **2018**, *138*, 1−7.

(16) Alves, L.; Pereira, V.; Lagarteira, T.; Mendes, A. Catalytic Methane Decomposition to Boost the Energy Transition: Scientific and Technological Advancements. *Renewable Sustainable Energy Rev.* **2021**, *137*, 110465.

(17) Puliyalil, H.; Laši Jurković, D.; Dasireddy, V. D. B. C.; Likozar, B. A Review of Plasma-Assisted Catalytic Conversion of Gaseous Carbon Dioxide and Methane into Value-Added Platform Chemicals and Fuels. *RSC Adv.* **2018**, *8*, 27481−27508.

(18) Lee, D. H.; Song, Y.-H.; Kim, K.-T.; Lee, J.-O. Comparative Study of Methane Activation Process by Different Plasma Sources. *Plasma Chem. Plasma Process.* **2013**, *33*, 647−661.

(19) Zhong, G.; Hofmann, S.; Yan, F.; Telg, H.; Warner, J. H.; Eder, D.; Thomsen, C.; Milne, W. I.; Robertson, J. Acetylene: A Key Growth Precursor for Single-Walled Carbon Nanotube Forests. *J. Phys. Chem. C* **2009**, *113*, 17321−17325.

(20) Sugime, H.; Noda, S. Cold-Gas Chemical Vapor Deposition to Identify the Key Precursor for Rapidly Growing Vertically-Aligned Single-Wall and Few-Wall Carbon Nanotubes from Pyrolyzed Ethanol. *Carbon* **2012**, *50*, 2953−2960.

(21) Shibuya, A.; Chen, G.; Miyoshi, A.; Futaba, D. N. Improving the Synthetic Efficiency of Single-Wall Carbon Nanotube Forests Using a Gas-Analysis-Designed Mixed Carbon Feedstock. *Carbon* **2020**, *170*, 59−65.

(22) Ning, G.; Wei, F.; Wen, Q.; Luo, G.; Wang, Y.; Jin, Y. Improvement of Fe/MgO Catalysts by Calcination for the Growth of Single- and Double-Walled Carbon Nanotubes. *J. Phys. Chem. B* **2006**, *110*, 1201−1205.

(23) Jašek, O.; Eliáš, M.; Zajíčková, L.; Kudrle, V.; Bublan, M.; Matějková, J.; Rek, A.; Buršík, J.; Kadlečíková, M. Carbon Nanotubes Synthesis in Microwave Plasma Torch at Atmospheric Pressure. *Mater. Sci. Eng., C* **2006**, *26*, 1189−1193.

(24) Jourdain, V.; Bichara, C. Current Understanding of the Growth of Carbon Nanotubes in Catalytic Chemical Vapour Deposition. *Carbon* **2013**, *58*, 2−39.

(25) Inaba, M.; Ochiai, T.; Ohara, K.; Kato, R.; Maki, T.; Ohashi, T.; Kawarada, H. Correlation between the Carbon Nanotube Growth Rate and Byproducts in Antenna-Type Remote Plasma Chemical Vapor Deposition Observed by Vacuum Ultraviolet Absorption Spectroscopy. *Small* **2019**, *15*, 1901504.

(26) Tsuji, T.; Shimizu, Y.; Kim, J.; Sakakita, H.; Hata, K.; Futaba, D. N.; Sakurai, S. A Mini-Microplasma-Based Synthesis Reactor for Growing Highly Crystalline Carbon Nanotubes. *Carbon* **2021**, *173*, 448−453.

(27) Schwach, P.; Pan, X.; Bao, X. Direct Conversion of Methane to Value-Added Chemicals over Heterogeneous Catalysts: Challenges and Prospects. *Chem. Rev.* **2017**, *117*, 8497−8520.

(28) Bajec, D.; Kostyniuk, A.; Pohar, A.; Likozar, B. Nonoxidative Methane Activation, Coupling, and Conversion to Ethane, Ethylene, and Hydrogen over Fe/HZSM-5, Mo/HZSM-5, and Fe−Mo/HZSM-5 Catalysts in Packed Bed Reactor. *Int. J. Energy Res.* **2019**, *43*, 6852−6868.

(29) Li, Y.; Chen, J.; Qin, Y.; Chang, L. Simultaneous Production of Hydrogen and Nanocarbon from Decomposition of Methane on a Nickel-Based Catalyst. *Energy Fuels* **2000**, *14*, 1188−1194.

(30) Zhang, R.; Zhang, Y.; Zhang, Q.; Xie, H.; Qian, W.; Wei, F. Growth of Half-Meter Long Carbon Nanotubes Based on Shulz-Flory Distribution. *ACS Nano* **2013**, *7*, 6156−6161.

(31) He, M.; Magnin, Y.; Jiang, H.; Amara, H.; Kauppinen, E. I.; Loiseau, A.; Bichara, C. Growth Modes and Chiral Selectivity of Single-Walled Carbon Nanotubes. *Nanoscale* **2018**, *10*, 6744−6750.

(32) Sadezky, A.; Muckenhuber, H.; Grothe, H.; Niessner, R.; Pöschl, U. Raman Microspectroscopy of Soot and Related Carbonaceous Materials: Spectral Analysis and Structural Information. *Carbon* **2005**, *43*, 1731−1742.

(33) Lavrov, B. P.; Melnikov, A. S.; Käning, M.; Röpcke, J. Uv Continuum Emission and Diagnostics of Hydrogen-Containing

Nonequilibrium Plasmas. *Phys. Rev. E: Stat. Phys., Plasmas, Fluids, Relat. Interdiscip. Top.* **1999**, *59*, 3526−3543.
(34) Phillips, D. M. Determination of Gas Temperature from Unresolved Bands in the Spectrum from a Nitrogen Discharge. *J. Phys. D: Appl. Phys.* **1976**, *9*, 507−521.
(35) Liu, C.; Cong, H. T.; Li, F.; Tan, P. H.; Cheng, H. M.; Lu, K.; Zhou, B. L. Semi-Continuous Synthesis of Single-Walled Carbon Nanotubes by a Hydrogen Arc Discharge Method. *Carbon* **1999**, *37*, 1865−1868.
(36) Wang, X. K.; Lin, X. W.; Mesleh, M.; Jarrold, M. F.; Dravid, V. P.; Ketterson, J. B.; Chang, R. P. H. The Effect of Hydrogen on the Formation of Carbon Nanotubes and Fullerenes. *J. Mater. Res.* **1995**, *10*, 1977−1983.

https://doi.org/10.1021/acsomega.1c01822
ACS Omega 2021, 6, 18763−18769